nature methods

ARTICLES

https://doi.org/10.1038/s41592-020-0782-3

A 6-nm ultra-photostable DNA FluoroCube for fluorescence imaging

Stefan Niekamp[1,2], Nico Stuurman[1,2] and Ronald D. Vale[1,2] ✉

Photobleaching limits extended imaging of fluorescent biological samples. We developed DNA-based 'FluoroCubes' that are similar in size to the green fluorescent protein, have single-point attachment to proteins, have a ~54-fold higher photobleaching lifetime and emit ~43-fold more photons than single organic dyes. We demonstrate that DNA FluoroCubes provide outstanding tools for single-molecule imaging, allowing the tracking of single motor proteins for >800 steps with nanometer precision.

Imaging proteins and macromolecular complexes at the single-molecule level is a powerful method to study distribution, stoichiometry, dynamics and precise motion of molecular machines[1]. To achieve high spatiotemporal resolution, proteins of interest are often labeled with fluorescent probes[1]. An ideal probe is photostable (long half-life), (continuously) bright, small and can be monovalently attached to biological molecules. While organic dyes[2,3] and fluorescent proteins[4] fulfill the last two criteria, they often suffer from photobleaching, which leads to a low signal. Alternative probes such as quantum dots[2,5] and other fluorescent nanoparticles[6] are very bright and extremely photostable, but frequently exhibit large fluctuations in intensity (blinking). Labeling with these probes is complicated by their relatively large size[2,3,5] (~15 nm; Supplementary Fig. 1a), which can perturb protein function and by the often-missing control over surface chemistry, which can lead to multiple proteins attaching to the same fluorescent probe[7].

We developed small (~6 nm) DNA-based FluoroCubes that have single-point attachment, exhibit continuous emission, emit up to ~43-fold more photons than single organic dyes and have an up to ~54-fold longer half-life than single organic dyes. We show that the photostability of the DNA FluoroCubes varies with the type of organic dye attached to the DNA. We also provide some preliminary insights into the mechanism(s) for the increased photostability of DNA FluoroCubes. Attaching these DNA FluoroCubes to the microtubule-based motor protein kinesin, we were able to track its movement for more than 800 steps with nanometer precision.

Results

Design and assembly of six-dye DNA FluoroCubes. Previous work established that placing organic dyes within 2 nm of each other results in quenching[7], while dye spacing of >5 nm results in a linear intensity increase with the number of dyes[8]. We were interested in the properties of probes separated by 2–5 nm.

To set the position of dyes with nanometer precision, we took advantage of tools from DNA nanotechnology[8–10]. Using the single-stranded tiles approach[11,12], we designed a DNA FluoroCube composed of four 16 base-pair (bp) long double-stranded DNA (dsDNA) helices labeled with six of the same organic dyes such as ATTO 488, ATTO 565, ATTO 647N, Cy3N (sulfonated Cy3), Cy3 or Cy5 (Fig. 1a,b and Supplementary Fig. 1b) separated by distances ranging from roughly 2 to 6 nm. We reserved one position for the placement of a functional tag such as HALO-ligand, benzylguanine (for the SNAP tag), thiol, biotin or amine to label proteins at specific locations (Fig. 1b).

Since small DNA nanostructures are difficult to assemble because of high electrostatic repulsion between the negatively charged DNA strands[13], we optimized the folding yield and determined the structural integrity of the DNA FluoroCubes after thermal annealing. Using agarose gel electrophoresis, we measured a folding yield of over 60% (Fig. 1c and Supplementary Fig. 1c) and found that only folding reactions that contained all four oligos assembled into DNA FlurorCubes (Supplementary Fig. 1d). Negative-stain transmission electron microscopy showed that DNA FluoroCubes assembled into the desired shape, with slight variations (Fig. 1d and Supplementary Figs. 1e and 2). In summary, the protocol for the assembly of DNA FluoroCubes is easy and optimized for high yield (Supplementary Protocol).

Photophysical properties of six-dye DNA FluoroCubes. Next, we examined the fluorescent properties of DNA FluoroCubes prepared with the commonly used fluorescent probe Cy3. We compared the Cy3 six-dye FluoroCube to a single Cy3 dye attached to dsDNA. Surface-immobilized samples were imaged by total internal reflection fluorescence (TIRF) microscopy (Fig. 1e–h, see Methods). To quantify photostability, we determined the time when 50% of all probes photobleached (half-life) and the total number of photons emitted. To quantify brightness, we measured the average number of photons per frame.

A single Cy3 dye conjugated to dsDNA or protein (streptavidin) (Supplementary Fig. 3) displayed a constant intensity followed by one-step photobleaching (Fig. 1f and Supplementary Fig. 4). However, the Cy3 six-dye FluoroCube was substantially more photostable than a single Cy3 dye bound to dsDNA (up to ~54-fold increase in half-life) (Fig. 1i,l), and sometimes even increased in brightness during the time of acquisition (Supplementary Fig. 4). For instance, after 99% of the single Cy3 dyes bleached, more than 80% of the Cy3 six-dye FluoroCubes were still in the 'on' state. The total number of photons per Cy3 six-dye FluoroCube was ~43-fold higher than for a single Cy3 dye bound to dsDNA (Fig. 1j,m; $1.29 \pm 0.06 \times 10^7$ photons for the Cy3 six-dye FluoroCube versus $3.1 \pm 0.5 \times 10^5$ photons for a single Cy3 dye bound to dsDNA, the latter being consistent with previous reports[14]). The Cy3 six-dye FluoroCubes also blinked less than the single Cy3 dye bound to dsDNA (Supplementary Fig. 5i). However,

[1]Department of Cellular and Molecular Pharmacology, University of California, San Francisco, San Francisco, CA, USA. [2]Howard Hughes Medical Institute, University of California, San Francisco, San Francisco, CA, USA. ✉e-mail: Ron.Vale@ucsf.edu

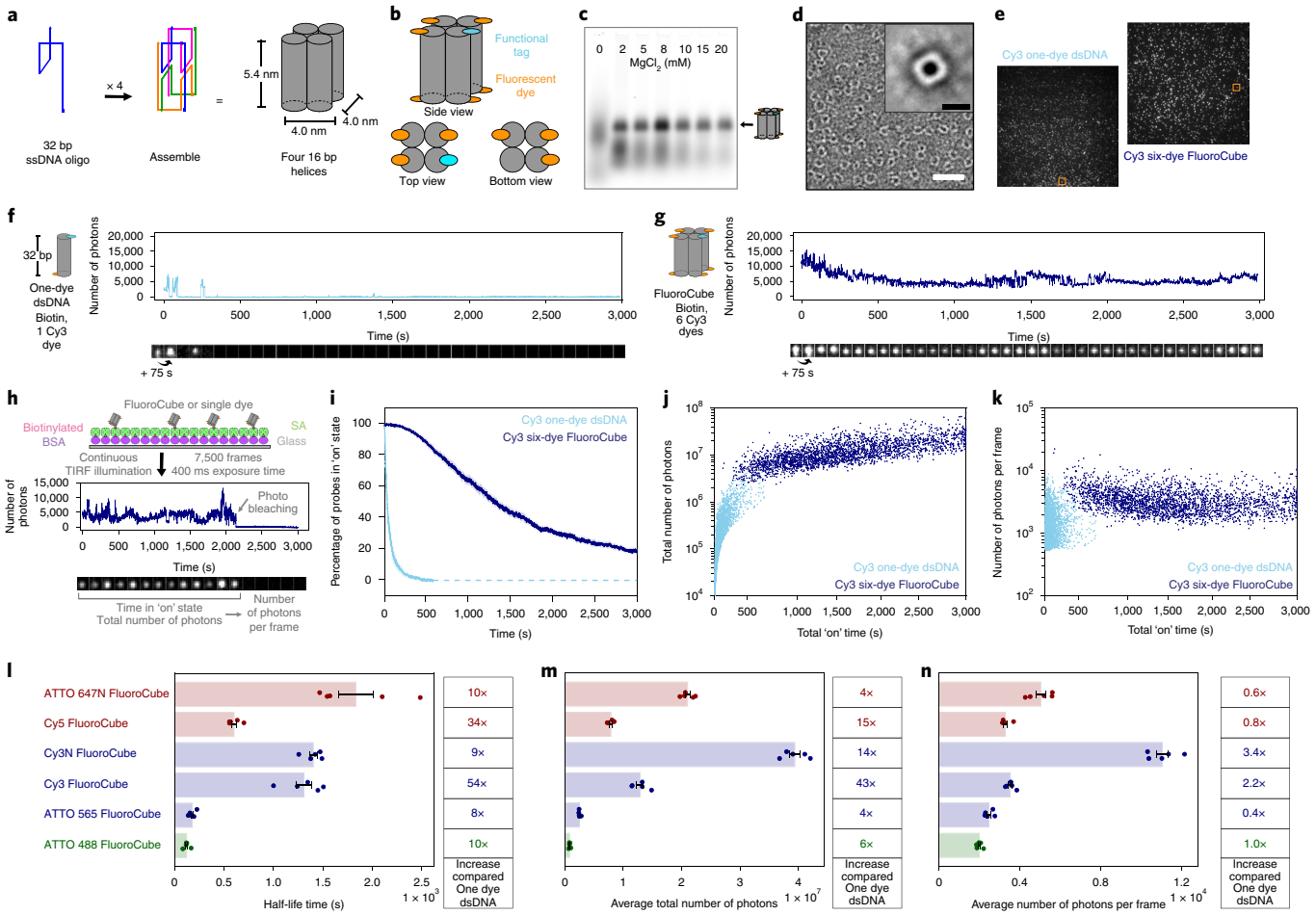

Fig. 1 | Design, assembly and photophysical properties of DNA FluoroCubes. a, Design and shape of DNA FluoroCubes. **b**, Cartoon depicting how each of the 5′ and 3′ ends of the DNA can be functionalized. For the six-dye FluoroCube design we used six fluorophores and one functional tag such as HALO-ligand, benzylguanine for SNAP tag, thiol, biotin or amine. **c**, 3.0% agarose gel of DNA FluoroCubes after thermal annealing. The four single-stranded (ss) DNA strands are annealed with different $MgCl_2$ concentrations. Quantification of assembly yield is shown in Supplementary Fig. 1c. Here the ssDNAs were modified with six ATTO 647N dyes and one biotin. **d**, Negative-stain electron microscopy image of DNA FluoroCubes. Inset shows class average of 983 particles. Here the DNA FluoroCube was labeled with six ATTO 647N dyes and one biotin. White scale bar, 30 nm; black scale bar, 6 nm. Class averaging was performed once. **e**, Example TIRF image of a biotin functionalized Cy3 six-dye FluoroCube and a 32 bp long dsDNA with one Cy3 dye. Orange boxes show molecules whose intensity traces are shown in **f** and **g**. Example intensity trace of Cy3 one-dye dsDNA (**f**) and Cy3 six-dye FluoroCube with one biotin (**g**). **h**, Experimental setup for quantification of photophysical properties of six-dye FluoroCubes and one-dye dsDNA. Intensity traces of single molecules are analyzed for time in 'on' state (half-life), total number of photons and number of photons per frame. **i**, Photostability of Cy3 six-dye FluoroCubes and Cy3 one-dye dsDNA. The survival rate was quantified by counting the percentage of probes in the 'on' state at any given time from 0 to 3,000 s. Opaque color is the standard error of the mean of five or four repeats (six-dye FluoroCubes or one-dye dsDNA, respectively) with more than 500 molecules each. Once all probes photobleached data analysis was terminated. This is indicated by the dashed line. **j**, Total number of photons of Cy3 six-dye FluoroCubes and Cy3 one-dye dsDNA as a function of the total 'on' time at the single-molecule level (pooled from all experiments). **k**, Average number of photons per frame of Cy3 six-dye FluoroCubes and Cy3 one-dye dsDNA as a function of the total 'on' time at the single-molecule level (pooled from all experiments). **l**–**n**, Bar plots of the half-life time (**l**), average of the total number of photons (**m**) and average number of photons per frame (**n**) of six-dye FluoroCubes with different fluorophores. The error bars show the standard error of the mean of five repeats with more than 100 molecules each. Dots show the values of individual experiments. The tables on the right show fold increase of six-dye FluoroCubes compared to one-dye dsDNA. **i**–**n**, Each experiment was repeated five or four times with freshly assembled six-dye FluoroCubes or one-dye dsDNA, respectively. For every experiment, we prepared new microscope slides. Exact numbers (also of the sample size) are given in Supplementary Tables 1 and 2. SA, Streptavidin; Cy3, nonsulfonated version of Cy3; Cy3N, sulfonated version of Cy3.

even though there are sixfold more dyes, the brightness of a Cy3 six-dye FluoroCubes was similar to a single Cy3 dye bound to dsDNA (Fig. 1k,n). With increasing light exposure, the photon output of Cy3 six-dye FluoroCubes behaved nonlinearly, as they plateaued in brightness at higher excitation powers (Supplementary Fig. 6b). In summary, Cy3 six-dye FluoroCubes emit an average of ~43-fold more photons than single Cy3 dyes but are similar in overall brightness.

We next tested the behavior of other dyes coupled to DNA FluoroCubes and found variable photophysical properties (Fig. 1l–n, Supplementary Figs. 5–7, Supplementary Movies 1–6 and Supplementary Table 1). The Cy5 six-dye, ATTO 647N six-dye and Cy3N six-dye FluoroCube also demonstrated a substantial increase in photostability (34-, 10- and 9-fold, respectively) (Fig. 1l and Supplementary Fig. 7a) and total number of photons (15-, 4- and 14-fold, respectively) (Fig. 1m and Supplementary Fig. 7b).

The ATTO 488 six-dye and ATTO 565 six-dye FluoroCubes were less photostable in absolute terms, but still showed a ten- and eightfold increase relative to single dyes attached to dsDNA (Fig. 1l and Supplementary Fig. 7a). Intermediate photostability was observed for the Janelia Fluorophores JF549 and JF646 six-dye FluoroCubes (ref. [15]) (Supplementary Fig. 8). As with the Cy3 six-dye FluoroCube, all of the six-dye FluoroCubes were similar in brightness to their respective single dyes (Fig. 1n). The various six-dye FluoroCubes performed better with oxygen scavengers[16] and triplet quenchers[17] (Supplementary Fig. 6d–f). However, even without these aids all six-dye FluoroCubes outperformed single dyes on dsDNA with oxygen scavengers[16] and triplet quenchers[17]. Taken together, the performance of the six-dye FluoroCubes is dye dependent, but all are substantially more photostable than commonly used single organic dyes (Fig. 1l–n) and some emit up to ~43-fold more photons than a single dye.

To further characterize our new fluorescent probes, we examined additional properties of the DNA FluoroCubes. Comparing the absorbance, excitation and emission spectra of various DNA FluoroCubes and their respective single dyes, we found a dye charge-dependent, large increase in absorbance in a 'shoulder' blue shifted from the main peak (Supplementary Fig. 9). This 'shoulder' absorbance is often observed for face-to-face dimers of dyes[18] and may result from the flexibility of DNA FluoroCubes in solution and the relatively long linker (up to 1.5 nm) between dye and oligo. An alternative explanation for the observed shoulder absorbance is that face-to-face dimers form between dyes on different DNA FluoroCubes. To test whether our DNA FluoroCubes are truly monomeric, we performed dynamic light scattering (DLS) and found that the measured diameters of different DNA FluoroCubes agree well with their predicted diameters (Supplementary Fig. 10). Moreover, the diameter distributions of the DNA FluoroCubes are symmetric (no shoulders visible) indicating that the DNA FluoroCubes are monodisperse in size. Additional experiments such as the measurement of the number of photobleaching steps (Supplementary Fig. 11) and our previous negative-stain imaging (Supplementary Fig. 2 and Supplementary Table 1) confirmed the DLS data. Thus, we concluded that six-dye FluoroCubes are predominantly monomeric and that the shoulder absorbance is likely caused by dyes on the same six-dye FluoroCube. The shoulder absorbance for six-dye FluoroCubes mainly represents nonfluorescent dyes (except for the Cy3 six-dye FluoroCube) as shown by comparing excitation and absorption spectra (Supplementary Figs. 9 and 12). Last, we measured fluorescence lifetime and fluorescence anisotropy (Supplementary Fig. 13), but did not find any change that might be correlated with increased photostability. Taken together, six-dye FluoroCubes are predominantly monomeric and present a dye charge-dependent 'shoulder' in absorbance that is blue shifted from the main peak.

Comparison of six-dye DNA FluoroCubes and quantum dots. Next, we compared the behavior of the ATTO 647N six-dye FluoroCubes to quantum dots that are known for their photostability. Quantum dots (655 Qdot nanocrystals) emitted about fourfold more photons than ATTO 647N six-dye FluoroCubes, were about fourfold brighter than ATTO 647N six-dye FluoroCubes and have a similar half-life time to ATTO 647N six-dye FluoroCubes (Supplementary Fig. 14c,d). However, quantum dots blink significantly more than six-dye FluoroCubes (Supplementary Fig. 14b). In addition, quantum dots tend to enter dark states in which they do not emit photons for a couple of seconds (Supplementary Fig. 14a), making it difficult to track quantum dots continuously. Moreover, quantum dots are significantly larger in size (10–20 nm) than the six-dye FluoroCubes[2,3,5] (Supplementary Fig. 1a) and typically not monovalent. In conclusion, six-dye FluoroCubes display much more stable and uniform fluorescence than quantum dots.

Insights into potential mechanism(s) of increased photostability of six-dye DNA FluoroCubes. To begin to understand the mechanism(s) behind the increase in photostability of the six-dye FluoroCubes, we investigated how the DNA scaffold might influence dye photophysics. A single dye on the same DNA FluoroCube scaffold (single dye cube) (Supplementary Fig. 15a) displayed a slight increase in photostability and emitted between around two- and tenfold more photons than corresponding one-dye dsDNA (Supplementary Fig. 15). Permuting through all six positions on the cube with a single Cy3N dye (Supplementary Fig. 16a), we noticed a higher photostability (about threefold longer half-life time) when the dye is attached to the 5′ end compared to the 3′ end of the same oligo (Supplementary Fig. 16). Together, these data show that the local environment of the DNA (single dye cube versus one-dye dsDNA) and the dye position (attachment linkage) can influence photostability.

To further investigate the effect of the geometry of dye placement on photostability, we compared the photostability of the Cy3 six-dye FluoroCubes to the same number of Cy3 dyes on an eightfold (by volume) larger structure (the previously described compact cube[13]), which places the dyes between ~6 and ~10 nm from one another (Supplementary Fig. 17a). The compact cube with one Cy3 dye behaved in a very similar way to a Cy3 single dye cube (Supplementary Fig. 17), while the compact cube with six Cy3 dyes had a slight increase in photostability but this was far less than the Cy3 six-dye FluoroCube. Thus, increasing the distances between the dyes from ~2–6 nm (six-dye FluoroCube) to ~6–10 nm (compact cube) decreases photostability, indicating the importance of distance between dyes for the photostability effect. We speculate that both direct dye interactions as well as resonance energy transfer between individual dyes in a six-dye FluoroCube play roles in this phenomenon (Supplementary Fig. 18), although additional work is required to fully understand the photophysical mechanisms underlying six-dye DNA FluoroCube photostability.

Tracking steps of a single kinesin over more than 6 µm. We next tested whether DNA FluoroCubes can be attached to proteins and used for prolonged readouts of activity. For this purpose, we labeled an ultraprocessive kinesin KIF1A[19] with a ATTO 647N six-dye FluoroCube using a C-terminal HALO-tag (Fig. 2a) and imaged it moving along axonemes. To ensure that a DNA FluoroCube labeled kinesin behaves in a similar way to a single dye labeled kinesin (single TMR HALO-dye), we compared velocity and processivity and found almost identical values indicating that DNA FluoroCubes do not interfere with protein function in this assay (Supplementary Fig. 19). Labeling kinesin with an ATTO 647N six-dye FluoroCube enabled us to record more than 800 steps of an individual motor with nanometer precision (Fig. 2a,b and Supplementary Movie 7). The trace in Fig. 2 revealed an on-axis step size of 7.8 nm with almost no off-axis stepping (Fig. 2d,e), which is in good agreement with previous reports[19,20] (discussion in Supplementary Fig. 20). Moreover, using ATTO 647N six-dye FluoroCubes allowed us to collect more than 6,000 data points of an individual motor compared to approximately 200 data points that can be collected at a similar resolution with a single organic dye[21,22]. By recording very long traces, we could detect occasional pausing and velocity fluctuations within the trace of an individual kinesin (Fig. 2c). Previous work demonstrated that different kinesins can have different velocities[23], but our prolonged observations showed that even individual kinesins undergo considerable velocity fluctuations over time.

Discussion

We developed small (~6-nm), ultra-photostable fluorescent probes. We have shown that six-dye FluoroCubes can emit up to 43-fold more photons and have an up to ~54-fold longer half-life than single organic dyes, making them ideal for long-term imaging. Comparing

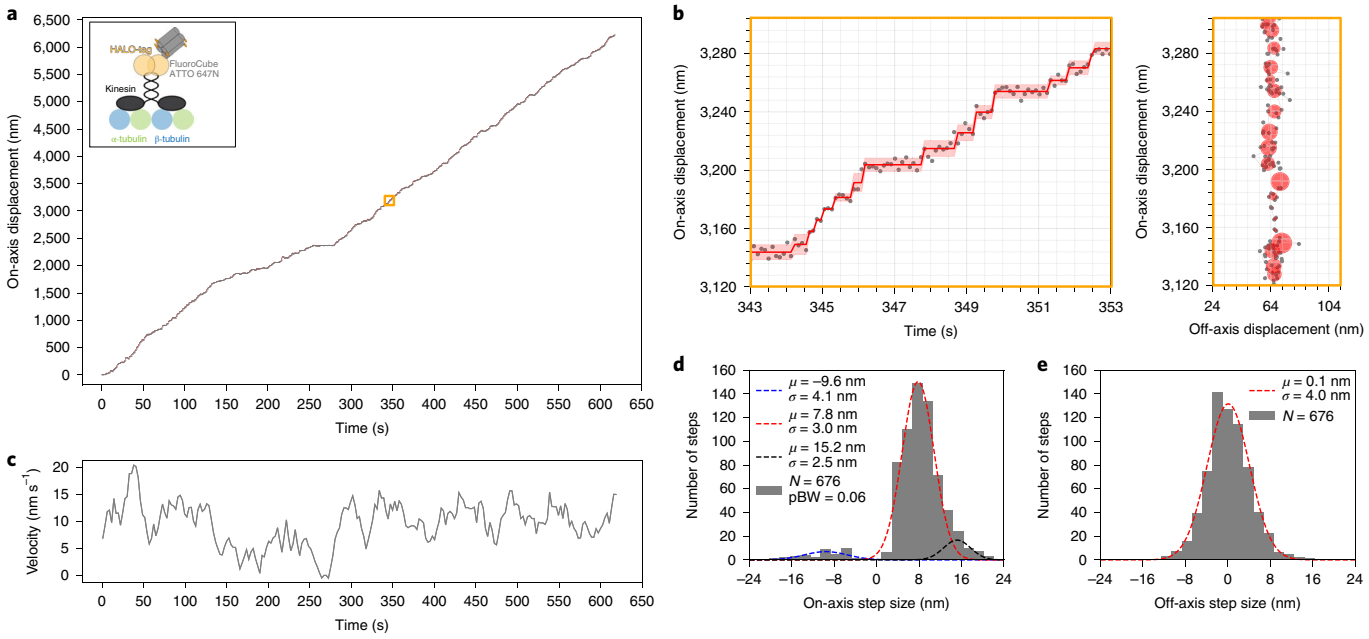

Fig. 2 | Tracking steps of a single kinesin over more than 6 µm. a, Raw stepping data with position versus time of one kinesin (gray dots) over 6 µm with detected steps (red line) along an axoneme. The opaque red line shows the standard deviation for each step. The insert shows the experimental setup for which a kinesin is labeled with one ATTO 647N six-dye FluoroCube with a HALO-tag (for details see Methods). Enlargement of the orange box is shown in **b**. The movement of this particular kinesin is shown in Supplementary Movie 7. **b**, Left, zoom-in on the raw stepping data with position versus time of a single kinesin as shown in **a**. Right, same trace as on the left but in *xy* space. The gray dots are raw data and the red circles show the fitted position for which the radius corresponds to the standard deviation. **c**, Velocity over time for the stepping trace of a single kinesin as shown in **a**. The gray line shows a moving average of velocity binned into 15.6 s (for details see Methods). **d**, Histogram of the on-axis step size distribution of the data shown in **a**. The data was split into positive and negative steps and fit with Gaussians. For the negative steps, a single Gaussian was used (blue) whereas for the positive steps two Gaussians were used (red, black). pBW is the fraction of backward steps. **e**, Histogram of the off-axis step size distribution of the data shown in **a** fitted with a single Gaussian. **d**,**e**, We detected 821 steps but only used 676 steps for further quantification because we only counted steps for which the step itself and the previous as well as following step had a standard deviation of less than 4 nm. **a**–**e**, All data shown here is from a single kinesin stepping trace (sample size $n=1$). However, we analyzed and quantified additional stepping traces of more motors and found very similar results (Supplementary Fig. 20).

six-dye FluoroCubes to single organic dyes, we found that the increase in photostability is dye specific. Currently, the ATTO 647N six-dye and Cy3N six-dye FluoroCubes demonstrate the most desirable properties, since they have the longest half-life and emit the most photons per probe (Fig. 1). Even the poorest performing six-dye FluoroCube (ATTO 488) has a tenfold longer half-life and emits sixfold more photons than a single organic dye. Quantum dots are fluorescence emitters with comparable long half-lives. However, quantum dots exhibit significantly more blinking than six-dye FluoroCubes, and their larger size and multivalent attachment[2,3,5] makes them more challenging to use as a noninvasive probe for protein activity. Applying the ATTO 647N six-dye FluoroCube to single-molecule imaging, we were able to track the movement of the motor protein kinesin with nanometer precision over more than 800 steps (Fig. 2) without any evidence of perturbation by the probe.

We investigated potential mechanism(s) that contribute to increased photostability of the six-dye FluoroCubes and found that the local environment of the DNA and the dye position (attachment linkage) influence photostability. We also found that increased photostability disappears when the spacing between dyes increases from ~2–6 nm (FluoroCubes) to ~6–10 nm (compact cubes[13]) in a similar DNA-based scaffold. Based on these observations, we speculate that resonance energy transfer between individual dyes in a six-dye FluoroCube contributes to the increased photostability. However, a more detailed understanding of the mechanism(s) for the increased photostability awaits further studies. It is also likely that further optimizations could be made to improve photostability. Based on our current work, we suggest that improvements could be achieved by using other dyes such as self-healing fluorophores[14], by adding DNA intercalating dyes[24], by increasing the number of fluorophores on the DNA FluoroCube[8], by changing the spacing between dyes (either by changing the cube size[7,13] or by alternating the dye linker length) or by changing the DNA sequence close to the fluorophores[25].

DNA FluoroCubes are easily prepared from commercially available reagents and can be attached to all commonly used protein tags, making them simple to use for in vitro studies. We anticipate that DNA FluoroCubes will become the reagent of choice for in vitro and extracellular single-molecule imaging experiments. Beyond single-molecule studies, the long photobleaching lifetime and high number of total photons of DNA FluoroCubes could prove useful in numerous other fluorescence imaging applications, including FISH[26], MERFISH[27], DNA-PAINT[28] or immunofluorescence for research and medical diagnosis.

Online content

Any methods, additional references, Nature Research reporting summaries, source data, extended data, supplementary information, acknowledgements, peer review information; details of author contributions and competing interests; and statements of data and code availability are available at https://doi.org/10.1038/s41592-020-0782-3.

Received: 25 July 2019; Accepted: 12 February 2020;
Published online: 16 March 2020

References

1. Joo, C., Balci, H., Ishitsuka, Y., Buranachai, C. & Ha, T. Advances in single-molecule fluorescence methods for molecular biology. *Annu. Rev. Biochem.* **77**, 51–76 (2008).
2. Resch-Genger, U., Grabolle, M., Cavaliere-Jaricot, S., Nitschke, R. & Nann, T. Quantum dots versus organic dyes as fluorescent labels. *Nat. Methods* **5**, 763–775 (2008).
3. Zheng, Q. et al. Ultra-stable organic fluorophores for single-molecule research. *Chem. Soc. Rev.* **43**, 1044–1056 (2014).
4. Shaner, N. C., Steinbach, P. A. & Tsien, R. Y. A guide to choosing fluorescent proteins. *Nat. Methods* **2**, 905–909 (2005).
5. Wichner, S. M. et al. Covalent protein labeling and improved single-molecule optical properties of aqueous CdSe/CdS quantum dots. *ACS Nano* **11**, 6773–6781 (2017).
6. Wolfbeis, O. S. An overview of nanoparticles commonly used in fluorescent bioimaging. *Chem. Soc. Rev.* **44**, 4743–4768 (2015).
7. Schröder, T., Scheible, M. B., Steiner, F., Vogelsang, J. & Tinnefeld, P. Interchromophoric interactions determine the maximum brightness density in DNA origami structures. *Nano Lett.* **19**, 1275–1281 (2019).
8. Woehrstein, J. B. et al. Sub–100-nm metafluorophores with digitally tunable optical properties self-assembled from DNA. *Sci. Adv.* **3**, e1602128 (2017).
9. Rothemund, P. W. K. Folding DNA to create nanoscale shapes and patterns. *Nature* **440**, 297–302 (2006).
10. Douglas, S. M. et al. Rapid prototyping of 3D DNA-origami shapes with caDNAno. *Nucleic Acids Res.* **37**, 5001–5006 (2009).
11. Ke, Y., Ong, L. L., Shih, W. M. & Yin, P. Three-dimensional structures self-assembled from DNA bricks. *Science* **338**, 1177–1183 (2012).
12. Wei, B., Dai, M. & Yin, P. Complex shapes self-assembled from single-stranded DNA tiles. *Nature* **485**, 623–626 (2012).
13. Scheible, M. B. et al. A compact DNA cube with side length 10 nm. *Small* **11**, 5200–5205 (2015).
14. Zheng, Q. et al. Electronic tuning of self-healing fluorophores for live-cell and single-molecule imaging. *Chem. Sci.* **8**, 755–762 (2017).
15. Grimm, J. B. et al. A general method to improve fluorophores for live-cell and single-molecule microscopy. *Nat. Methods* **12**, 244–250 (2015).
16. Aitken, C. E., Marshall, R. A. & Puglisi, J. D. An oxygen scavenging system for improvement of dye stability in single-molecule fluorescence experiments. *Biophys. J.* **94**, 1826–1835 (2008).
17. Rasnik, I., McKinney, S. A. & Ha, T. Nonblinking and long-lasting single-molecule fluorescence imaging. *Nat. Methods* **3**, 891–893 (2006).
18. Nicoli, F. et al. Proximity-induced H-aggregation of cyanine dyes on DNA-duplexes. *J. Phys. Chem. A* **120**, 9941–9947 (2016).
19. Tomishige, M., Klopfenstein, D. R. & Vale, R. D. Conversion of Unc104/KIF1A kinesin into a processive motor after dimerization. *Science* **297**, 2263–2267 (2002).
20. Okada, Y., Higuchi, H. & Hirokawa, N. Processivity of the single-headed kinesin KIF1A through biased binding to tubulin. *Nature* **424**, 574–577 (2003).
21. Yildiz, A., Tomishige, M., Vale, R. D. & Selvin, P. R. Kinesin walks hand-over-hand. *Science* **303**, 676–678 (2004).
22. Stepp, W. L., Merck, G., Mueller-Planitz, F. & Ökten, Z. Kinesin-2 motors adapt their stepping behavior for processive transport on axonemes and microtubules. *EMBO Rep.* **18**, 1947–1956 (2017).
23. Reddy, B. J. N. et al. Heterogeneity in kinesin function. *Traffic* **18**, 658–671 (2017).
24. Ozhalici-Unal, H. & Armitage, B. A. Fluorescent DNA nanotags based on a self-assembled DNA tetrahedron. *ACS Nano* **3**, 425–433 (2009).
25. Kretschy, N., Sack, M. & Somoza, M. M. Sequence-dependent fluorescence of Cy3- and Cy5-labeled double-stranded DNA. *Bioconjug. Chem.* **27**, 840–848 (2016).
26. Femino, A. M., Fay, F. S., Fogarty, K. & Singer, R. H. Visualization of single RNA transcripts in situ. *Science* **280**, 585–590 (1998).
27. Chen, K. H., Boettiger, A. N., Moffitt, J. R., Wang, S. & Zhuang, X. RNA imaging. Spatially resolved, highly multiplexed RNA profiling in single cells. *Science* **348**, aaa6090 (2015).
28. Jungmann, R. et al. Multiplexed 3D cellular super-resolution imaging with DNA-PAINT and Exchange-PAINT. *Nat. Methods* **11**, 313–318 (2014).

Methods

Flow-cell preparation. Flow cells were assembled as previously described[29]. Briefly, we made custom three-cell flow chambers using laser-cut double-sided adhesive sheets (Soles2dance, 9474-08x12-3M 9474LE 300LSE), glass slides (Thermo Fisher Scientific, 12-550-123) and 170 µm thick coverslips (Zeiss, 474030-9000-000). The coverslips were cleaned in a 5% v/v solution of Hellmanex III (Sigma, Z805939-1EA) at 50 °C overnight and washed extensively with Milli-Q water afterward.

Assembly and analysis of DNA FluoroCubes, single dye cubes, dsDNA and compact cubes. For each six-dye FluoroCube and single dye cube (FluoroCube with a single dye) four 32 bp long oligonucleotide strands are required, each modified either with dyes or a functional tag such as biotin or HALO-ligand[30] (Supplementary Fig. 1b and Supplementary Tables 3 and 4). These four oligos are connected using crossovers resulting in four connected 16 bp long dsDNAs with a size of approximately 5.4 × 4.0 × 4.0 nm. A detailed map of oligonucleotide routing and the bases is depicted in Supplementary Fig. 1b. Two oligos were used for the dsDNA with one dye and 28 oligos were used for the compact cubes[13] (Supplementary Tables 3 and 4). For each of the four samples, oligos were mixed to a final concentration of 10 µM (if not stated otherwise) in folding buffer (5 mM Tris pH 8.5, 1 mM EDTA and 40 mM $MgCl_2$ (if not stated otherwise)) and annealed by denaturation at 85 °C for 5 min followed by cooling from 80 to 65 °C with a decrease of 1 °C per 5 min. Afterward, the samples were further cooled from 65 to 25 °C with a decrease of 1 °C per 20 min and then held at 4 °C. Folding products were analyzed by 3.0% agarose gel electrophoresis (if not stated otherwise) in TBE (45 mM Tris-borate and 1 mM EDTA) with 12 mM $MgCl_2$ at 70 V for 2.5 h on ice and purified by extraction and centrifugation in Freeze'N Squeeze columns (Bio-Rad Sciences, 732-6165). The gels were scanned using a Typhoon 9400 scanner (GE Healthcare). A step-by-step protocol on DNA FluoroCube assembly can be found in the Supplementary Protocol and on protocols.io (https://doi.org/10.17504/protocols.io.8k2huye)[31].

Agarose gel-based yield estimation was carried out using ImageJ[32]. The percentage of DNA FluoroCubes that ran as a monomeric band was estimated as the background-subtracted integrated intensity value divided by the background-subtracted integrated intensity value enclosing the material from the well, down to the bottom of the leading band (single oligos). Note, that the different brightness of FluoroCube bands in the agarose gels is mainly due to the variation of material loaded into the gel.

Negative-stain electron microscopy data collection and processing. For negative-stain transmission electron microscopy, unpurified, but folded DNA FluoroCubes at 300 nM (diluted in FluoroCube Buffer: 20 mM Tris pH 8.0, 1 mM EDTA, 20 mM Mg-Ac and 50 mM NaCl) were incubated on freshly glow discharged carbon coated 400 mesh copper grids for 1 min and blotted off. Immediately after blotting, a 0.75% uranyl formate solution was applied for staining and blotted off without incubation. This staining was repeated four times and followed by a last incubation for which the stain was incubated for 45 s before blotting. Samples were allowed to air dry before imaging. Data were acquired at University of California, San Francisco (UCSF), on a Tecnai T12 microscope operating at 120 kV, using a 4,000 × 4,000 charge-coupled device (CCD) camera (UltraScan 4000, Gatan) and a pixel size of 1.7 Å per pixel. For the class average in Fig. 1d, 1,743 particles were picked and boxed using EMAN 2.21 (ref. [33]). Then a two-dimensional classification was performed to remove junk and noisy particles, leading to 983 particles being selected.

Mono-Q clean-up of DNA FluoroCubes. Thermally annealed DNA FluoroCubes were purified using anion exchange chromatography with a GE Source 15Q 4.6/100 PE column (Supplementary Fig. 2l). DNA FluoroCubes were bound to the column in Buffer A (20 mM Tris pH 8.0, 1 mM EDTA, 10 mM Mg-Ac and 10% glycerol) and afterward, the ionic strength was increased linearly by adding Buffer B (20 mM Tris pH 8.0, 2 M K-Ac, 1 mM EDTA, 10 mM Mg-Ac and 10% glycerol) to 100% over 80 min.

Labeling of oligonucleotides with Janelia Fluorophores. We mixed 5′ and 3′ amino modified oligos (Supplementary Table 3) at a final concentration of 500 µM (in water) with NHS ester modified Janelia Fluorophores JF549 or JF646 (ref. [15]) at a final concentration of 5 mM (in DMSO) in 15 mM HEPES pH 8.5 buffer. These solutions were incubated for 4 h at room temperature. We then removed excess dye by four subsequent spins of the solution over Micro Bio-Spin 6 Columns (Bio-Rad) at 700*g* for 2 min. The final oligo concentration was determined with an ultraviolet spectrophotometer. Afterward, six-dye FluoroCubes were assembled as described before.

Preparation of flow cells with DNA FluoroCubes, single dye cubes, dsDNA, compact cubes, biotinylated dyes and quantum dots. The preparation of flow cells is identical for six-dye cubes (six-dye FluoroCubes), single-dye cubes (FluoroCubes with a single dye), the dsDNA with one dye, biotinylated dyes and the one- and six-dye compact cubes[13]. In all cases, samples were folded with biotin as the functional tag (except the single, biotinylated dye) and we used unpurified, but folded samples. We first added 10 µl of 5 mg ml^{-1} Biotin-BSA (Thermo Scientific, 29130) in BRB80 to the flow-cell and incubated for 2 min. Afterward, we added another 10 µl of 5 mg ml^{-1} Biotin-BSA in BRB80 and incubated for 2 min. Then we washed with 20 µl of FluoroCube Buffer (20 mM Tris pH 8.0, 1 mM EDTA, 20 mM Mg-Ac and 50 mM NaCl) with 2 mg ml^{-1} β-casein (Sigma, C6905), 0.4 mg ml^{-1} κ-casein (Sigma, C0406). This was followed by addition of 10 µl of 0.5 mg ml^{-1} Streptavidin (Vector Laboratories, SA-5000) in PBS (pH 7.4) and a 2 min incubation. We then washed with 20 µl of FluoroCube Buffer with 2 mg ml^{-1} β-casein and 0.4 mg ml^{-1} κ-casein. Next, we added either DNA-based samples or the single, biotinylated dye in FluoroCube Buffer or quantum dots (Qdot 655 Streptavidin Conjugate, ThermoFisher Scientific, Q10121MP) and incubated for 5 min. Finally, we washed with 30 µl of FluoroCube Buffer with 2 mg ml^{-1} β-casein and 0.4 mg ml^{-1} κ-casein. We then added the protocatechuic acid (PCA)/protocatechuate-3,4-dioxygenase (PCD)/Trolox oxygen scavenging system[16,17] in FluoroCube Buffer with 2 mg ml^{-1} β-casein, and 0.4 mg ml^{-1} κ-casein for the DNA-based samples and or the single, biotinylated dye. For the quantum dots we added the PCA/PCD oxygen scavenging system[16] and 1% β-mercaptoethanol in FluoroCube Buffer with 2 mg ml^{-1} β-casein and 0.4 mg ml^{-1} κ-casein.

We note that the concentration of the PCA/PCD/Trolox oxygen scavenging system[16,17] is critical and small deviations had large effects on the performance of all samples used in our experiments. We used the following concentrations in all our experiments: 2.5 mM of PCA (Sigma, 37580) at pH 9.0, 5 U of PCD (Oriental Yeast Company Americas Inc., 46852004) and 1 mM Trolox (Sigma, 238813) at pH 9.5.

Measurements of fluorescence anisotropy, fluorescence lifetime, as well as absorption, excitation and emission spectra. We determined fluorescence anisotropy, fluorescence lifetime, as well as excitation and emission spectra using an ISS K2 multifrequency fluorometer in bulk measurements. All experiments were performed at room temperature (21–23 °C). Instrument settings for the excitation and emission spectra are listed in Supplementary Table 5, settings for the fluorescence anisotropy measurements are listed in Supplementary Table 6 and settings for the fluorescence lifetime measurements are listed in Supplementary Table 7. For the absorption spectra we used an Eppendorf Spectrophotometer (ultraviolet-visible spectrum BioSpectrometer) and measured the absorbance from 240 to 800 nm. For all samples we used a concentration of 500 nM. In addition, we normalized the absorption spectra based on the 260 nm absorbance.

DLS of DNA FluoroCubes and compact cubes. Dynamic light scattering (DLS) measurements were performed using a Zetasizer ZS90 (Malvern Panalytical) at a wavelength of 633 nm. Sixty microliters of unpurified DNA FluoroCubes or compact cubes were measured at 25 °C at a concentration of 5 µM in FluoroCube Buffer (20 mM Tris pH 8.0, 1 mM EDTA, 20 mM Mg-Ac and 50 mM NaCl).

Kinesin cloning, purification and labeling. The kinesin construct was cloned and purified as previously described[19] except that the green fluorescent protein was replaced with a HALO-tag[30].

The plasmid was transfected and expressed in Agilent BL21(DE3) cells. Cells were grown in LB at 37 °C until they reached 1.0 optical density (OD_{600}) and the expression was induced by addition of 0.2 mM IPTG. Then the cells were incubated overnight at 20 °C. Cells were pelleted and gathered in lysis buffer (25 mM Pipes (pH 6.8), 2 mM $MgCl_2$, 250 mM NaCl, 20 mM imidazole, 1 mM BME, 0.1 mM ATP and 0.4 mM PMSF) and lysed in the EmulsiFlex homogenizer (Avestin). After a spin in a Sorvall SS-34 rotor for 30 min at 30,000*g*, the supernatant was loaded onto a Ni-NTA resin (QIAGEN, 30210) and washed with additional lysis buffer. We then took 500 µl of beads slur in lysis buffer supplemented with 10 mM $MgCl_2$ and added either ATTO 647N six-dye FluoroCubes with a HALO-tag[30] to 5 µM final or 5 µM final of HALO-tag TMR dye (Promega). These mixtures were incubated on a Nutator for 3 h at 4 °C. Afterward, we washed with additional lysis buffer supplemented with 10 mM $MgCl_2$. Then the protein of both labeling reactions was eluted by adding 300 mM of imidazole to the lysis buffer supplemented with 10 mM $MgCl_2$. Subsequently the samples were purified by gel filtration over a S200 10/300GL column from GE Healthcare. Gel filtration buffer was composed of 25 mM Pipes (pH 6.8), 10 mM $MgCl_2$, 200 mM NaCl, 1 mM EGTA, 1 mM DTT and 10% sucrose. Finally, the samples were flash frozen and stored at −80 °C.

Preparation of flow cells with kinesin. Single-molecule assays with kinesin in flow cells were prepared as previously described[19,21]. We first added 10 µl of Alexa 488 labeled axonemes in BRB80 (80 mM Pipes (pH 6.8), 1 mM $MgCl_2$, 1 mM EGTA) and incubated for 5 min. Then, we washed with 60 µl of BRB80 with 1.0 mg ml^{-1} κ-casein (Sigma, C0406) supplemented with 5 mM $MgCl_2$. For the comparison between ATTO 647N six-dye FluoroCubes labeled kinesin and HALO-tag TMR dye labeled kinesin, we added 10 µl of labeled motor in BRB80 with additional 5 mM $MgCl_2$, 1.0 mg ml^{-1} κ-casein, 1 mM ATP and the PCA/PCD/Trolox oxygen scavenging system[16,17]. For the high-resolution stepping data acquisition, we added 10 µl of ATTO 647N six-dye FluoroCubes labeled kinesin in BRB80 with additional 5 mM $MgCl_2$, 1.0 mg ml^{-1} κ-casein, 1.5 µM ATP, an ATP regeneration system (1 mM phosphoenolpyruvate (Sigma, 860077), ~0.01 U pyruvate kinase (Sigma, P0294), ~0.02 U lactate dehydrogenase (Sigma, P0294)) and the PCA/PCD/Trolox oxygen scavenging system[16,17].

Microscope setup. All data collections were carried out at room temperature (~23 °C) using a TIRF inverted microscope (Nikon Eclipse Ti microscope) equipped with a 100× (1.45 numerical aperture) oil objective (Nikon, Plan Apo ϡ). We used an Andor iXon 512 × 512 pixel electron-multiplying camera, DU-897E

and a pixel size of 159 nm. We used two stepping motor actuators (Sigma Koki, SGSP-25ACTR-B0) mounted on a KS stage (KS, Model KS-N) and a custom-built cover to reduce noise from air and temperature fluctuations. A reflection-based autofocus unit (FocusStat4) was custom adapted to our microscope (Focal Point Inc.). For the data collection we used a 488 nm laser (Coherent Sapphire 488 LP, 150 mW), a 561 nm laser (Coherent Sapphire 561 LP, 150 mW) and a 640 nm laser (Coherent CUBE 640-100C, 100 mW). A TIRF cube containing excitation filter (Chroma, zet405/491/561/638×), dichroic mirror (zt405/488/561/638rpc), and emission filter (Chroma, zet405/491/561/647m) was mounted in the upper turret of the microscope. The lower turret contained an ET450/50m (Chroma) filter for the 488 nm laser, an ET600/50m (Chroma) filter for the 561 nm laser and an ET700/75m (Chroma) filter for the 640 nm laser.

Single-molecule TIRF data collection and analysis of DNA FluoroCubes, single dye cubes, dsDNA, biotinylated dyes, compact cubes and quantum dots. The TIRF data of surface-immobilized six-dye FluoroCubes, single dye cubes (FluoroCubes with a single dye), dsDNA with one dye, biotinylated dyes, quantum dots or one- and six-dye compact cubes[13] was acquired under continuous laser illumination with an intensity (irradiance) of 120 W cm^{-2} (488 nm laser), 120 W cm^{-2} (561 nm laser) and 160 W cm^{-2} (640 nm laser) and an exposure of 400 ms if not specified otherwise. The acquisition length varied based on the experiment and how fast the respective probe bleached. Thus, before conducting an experiment we preestablished the acquisition length. Typically, we either recoded 7,500 frames (3,000 s), 2,000 frames (800 s), 1,500 frames (600 s) or 300 frames (120 s). We used the camera in conventional charge-coupled device (CCD) mode (that is, no electron-multiplying gain). All datasets were acquired with a '16 bit, conventional, 3 MHz' setting and a preamp gain of 5×. All experiments were performed at room temperature (21–23 °C). The acquisition software was µManager[34] 2.0 and data was analyzed in ImageJ[32]. Single molecules were located and traced using the Spot Intensity Analysis plugin in ImageJ[32] (https://imagej.net/Spot_Intensity_Analysis) with the following settings: time interval of 0.4 s (except for data in Supplementary Fig. 6 for which the exposure time was used as listed in Supplementary Table 8), electron per analog-to-digital unit (ADU) of 1.84, spot radius of 3, noise tolerance of 100 (except for the Cy3 one-dye dsDNA and the single, biotinylated Cy3 dye for which we used a noise tolerance of 50) and a median background estimation. The number of frames to check is shown in Supplementary Table 9 since it varies for each sample depending on how fast they bleach. Afterward, the data were further analyzed and plotted with a custom written Python script and only localized particles with >500 photons were counted as in the 'on' state. Note, that in some cases the average total number of photons is an underestimate since not all samples fully bleached within the acquisition time.

Single-molecule TIRF data collection and analysis of kinesin stepping. For the comparison between ATTO 647N six-dye FluoroCubes labeled kinesin and HALO-tag TMR dye labeled kinesin, the motors were continuously illuminated with an effective exposure time of 0.103 s with a 640 nm laser (160 W cm^{-2}) or a 561 nm laser (120 W cm^{-2}), respectively.

For the high-resolution stepping data acquisition, kinesins labeled with ATTO 647N six-dye FluoroCubes with a HALO-tag[30] were continuously illuminated with a 640 nm laser (160 W cm^{-2}) with an effective exposure time of 0.103 s. We used the camera in conventional CCD mode (that is, no electron-multiplying gain). All datasets were acquired with a '16 bit, conventional, 3 MHz' setting and a preamp gain of 5×. All experiments were performed at room temperature (21–23 °C). The acquisition software was µManager[34] 2.0. All emitters were fitted and localized using µManager's[34] 'Localization Microscopy' plugin as previously described[29]. Parameters for analysis are shown in Supplementary Table 10. Tracks of individual motors were extracted using µManager's[34] Localization Microscopy plugin. We set the minimum frame number to 1,000, the maximum number of missing frames to 100, the maximum distance between frames to 100 nm and the total minimum distances of the full track to 500 nm. Then tracks of individual motors were rotated using a principal component analysis implemented in Python. Afterward, we used a custom MATLAB (R, 2016b) script to identify individual steps using Chung Kennedy edgedetecting algorithm as previously described[35] and further analyzed the data in a custom written Python script. Only steps for which the step itself and the previous as well as following step had a standard deviation of less than 4 nm were considered for further quantification. The velocity over time for the stepping trace of a single kinesin was analyzed with a moving average for which we first binned the data into 2.6-s bins and then grouped six of these 2.6-s bins into 15.6-s bins. We used these 15.6-s bins to calculate the average velocity at any given point, but used the 2.6-s intervals to move along the time axis.

Figure preparation. Figures and graphs were created using ImageJ[32] (light microscopy data), Affinity designer (v.1.6.1, Serif (Europe) Ltd) and Python (v.2.7, Python Software Foundation).

Statistics. For each result the inherent uncertainty due to random or systematic errors and their validation are discussed in the relevant sections of the manuscript. Details about the sample size, number of independent calculations and the determination of error bars in plots are included in the figures and figure captions.

Reporting Summary. Further information on research design is available in the Nature Research Reporting Summary linked to this article.

Data availability

Example raw datasets of DNA FluoroCubes with six dyes, single dye cubes (FluoroCubes with a single dye), one-dye dsDNA constructs, single, biotinylated dyes and compact cubes used to determine the photophysical properties are hosted on Zenodo: https://doi.org/10.5281/zenodo.3561024 (ref. [36]). All other data files are available from the authors upon request.

Code availability

µManager acquisition and analysis software is available partly under the Berkeley Software Distribution license, partly under the GNU Lesser General Public License and development is hosted on GitHub at https://github.com/nicost/micro-manager. The latest version for MacOS and Windows can be downloaded here: https://micro-manager.org/wiki/Download%20Micro-Manager_Latest%20Release (v.2.0 gamma). The custom written Python code used to determine the total number of photons, the average number of photons per frame, and the half-life (photostability) for all fluorescent samples used in this study is hosted on Zenodo at https://doi.org/10.5281/zenodo.3629746 (ref. [37]). All other code is available from the authors upon request.

References

29. Niekamp, S. et al. Nanometer-accuracy distance measurements between fluorophores at the single-molecule level. *Proc. Natl Acad. Sci. USA* **116**, 4275–4284 (2019).
30. Los, G. V. et al. HaloTag: a novel protein labeling technology for cell imaging and protein analysis. *ACS Chem. Biol.* **3**, 373–382 (2008).
31. Niekamp, S., Stuurman, N. & Ronald, D. Folding of FluoroCubes v.1 (protocols.io.8k2huye, 2019); https://doi.org/10.17504/protocols.io.8k2huye
32. Schneider, C. A., Rasband, W. S. & Eliceiri, K. W. NIH Image to ImageJ: 25 years of image analysis. *Nat. Methods* **9**, 671–675 (2012).
33. Tang, G. et al. EMAN2: an extensible image processing suite for electron microscopy. *J. Struct. Biol.* **157**, 38–46 (2007).
34. Edelstein, A., Amodaj, N., Hoover, K., Vale, R. & Stuurman, N. Computer control of microscopes using µManager. *Curr. Protoc. Mol. Biol.* Ch.14, Unit14.20 (2010).
35. Qiu, W. et al. Dynein achieves processive motion using both stochastic and coordinated stepping. *Nat. Struct. Mol. Biol.* **19**, 193–200 (2012).
36. Niekamp, S., Stuurman, N. & Vale, R. D. *A 6-nm Ultra-Photostable DNA FluoroCube for Fluorescence Imaging* (Zenodo, 2019); https://doi.org/10.5281/ZENODO.3561024
37. Niekamp, S., Stuurman, N. & Vale, R. D. *Python code for a 6-nm Ultra-Photostable DNA FluoroCube for Fluorescence Imaging* (Zenodo, 2020); https://doi.org/10.5281/zenodo.3629746

Acknowledgements

We are grateful to J. Sung (UCSF) for critical discussions of the manuscript. We thank D. Mullins (UCSF) for teaching us how to use the ISS K2 multifrequency fluorometer. We are thankful to Y.-W. Jun and Y. Zhao (UCSF) for teaching us how to use the Malvern Zetasizer ZS90. We thank L. Lavis (Janelia Research Campus) for the suggestion of comparing sulfonated versus nonsulfonated dyes and for providing the JF549 and JF646 dyes. We are thankful to S. Douglas (UCSF) and A.G. York (Calico Laboratories) for feedback on the manuscript after preprinting. A. Carter (MRC Laboratory of Molecular Biology) and E. Villa (UCSD) supplied the MATLAB script for step detection of kinesin. We acknowledge funding from the National Institutes of Health grant nos. R01GM097312 and 1R35GM118106 (to R.D.V. and S.N.), and the Howard Hughes Medical Institute (to R.D.V., S.N. and N.S.).

Author contributions

S.N., N.S. and R.D.V. designed the research. S.N. prepared samples, collected TIRF microscopy data and electron microscopy data and analyzed it. S.N., N.S. and R.D.V. wrote the article. All authors read and commented on the paper.

Competing interests

The authors declare no competing interests.

Additional information

Supplementary information is available for this paper at https://doi.org/10.1038/s41592-020-0782-3.

Correspondence and requests for materials should be addressed to R.D.V.

Peer review information Rita Strack was the primary editor on this article and managed its editorial process and peer review in collaboration with the rest of the editorial team.

Reprints and permissions information is available at www.nature.com/reprints.

nature research

Corresponding author(s): Ronald D. Vale

Last updated by author(s): 02/04/2020

Reporting Summary

Nature Research wishes to improve the reproducibility of the work that we publish. This form provides structure for consistency and transparency in reporting. For further information on Nature Research policies, see Authors & Referees and the Editorial Policy Checklist.

Statistics

For all statistical analyses, confirm that the following items are present in the figure legend, table legend, main text, or Methods section.

n/a	Confirmed	
☐	☒	The exact sample size (*n*) for each experimental group/condition, given as a discrete number and unit of measurement
☐	☒	A statement on whether measurements were taken from distinct samples or whether the same sample was measured repeatedly
☒	☐	The statistical test(s) used AND whether they are one- or two-sided *Only common tests should be described solely by name; describe more complex techniques in the Methods section.*
☒	☐	A description of all covariates tested
☒	☐	A description of any assumptions or corrections, such as tests of normality and adjustment for multiple comparisons
☐	☒	A full description of the statistical parameters including central tendency (e.g. means) or other basic estimates (e.g. regression coefficient) AND variation (e.g. standard deviation) or associated estimates of uncertainty (e.g. confidence intervals)
☒	☐	For null hypothesis testing, the test statistic (e.g. *F*, *t*, *r*) with confidence intervals, effect sizes, degrees of freedom and *P* value noted *Give P values as exact values whenever suitable.*
☒	☐	For Bayesian analysis, information on the choice of priors and Markov chain Monte Carlo settings
☒	☐	For hierarchical and complex designs, identification of the appropriate level for tests and full reporting of outcomes
☐	☒	Estimates of effect sizes (e.g. Cohen's *d*, Pearson's *r*), indicating how they were calculated

Our web collection on statistics for biologists contains articles on many of the points above.

Software and code

Policy information about availability of computer code

Data collection	μManager acquisition and analysis software is available partly under the Berkeley Software Distribution (BSD) license, partly under the GNU Lesser General Public License (LGPL) and development is hosted on GitHub at https://github.com/nicost/micro-manager. The latest version for MacOS and Windows can be downloaded here: https://micro-manager.org/wiki/Download%20Micro-Manager_Latest%20Release (version 2.0 gamma). The custom written Python code used to determine the total number of photons, the average number of photons per frame, and the half-life (photostability) for all fluorescent samples used in this study is hosted on Zenodo: https://doi.org/10.5281/zenodo.3629746. All other code is available from the authors upon request.
Data analysis	Data was analyzed with and graphs were created using ImageJ29 (light microscopy data), Affinity designer (version 1.6.1, Serif (Europe) Ltd) and Python (version 2.7, Python Software Foundation).

For manuscripts utilizing custom algorithms or software that are central to the research but not yet described in published literature, software must be made available to editors/reviewers. We strongly encourage code deposition in a community repository (e.g. GitHub). See the Nature Research guidelines for submitting code & software for further information.

Data

Policy information about availability of data

All manuscripts must include a data availability statement. This statement should provide the following information, where applicable:

- Accession codes, unique identifiers, or web links for publicly available datasets
- A list of figures that have associated raw data
- A description of any restrictions on data availability

Example raw datasets of DNA FluoroCubes with six dyes, Single Dye Cubes, one dye double-stranded DNA constructs, single, biotinylated dyes, and Compact Cube used to determine the photophysical properties are hosted on Zenodo: https://doi.org/10.5281/zenodo.3561024. All other data files are available from the authors upon request.

Field-specific reporting

Please select the one below that is the best fit for your research. If you are not sure, read the appropriate sections before making your selection.

☒ Life sciences ☐ Behavioural & social sciences ☐ Ecological, evolutionary & environmental sciences

For a reference copy of the document with all sections, see nature.com/documents/nr-reporting-summary-flat.pdf

Life sciences study design

All studies must disclose on these points even when the disclosure is negative.

Sample size	We did not perform any sample size calculation as this is a methods paper. However, we ensured that the number of data points collected is adequate to demonstrate the usefulness of our new method.
Data exclusions	We pre-established the fitting parameters for the localization of single particles with preliminary experiments. Thus, when fitting single particles (FluoroCubes) with the Localization Plug-in we used the criteria as described in the Online Methods (see: "Single-molecule TIRF data collection and analysis of DNA FluoroCubes, Single Dye Cubes, double-stranded DNA, biotinylated dyes, Compact Cubes and quantum dots"). For the subsequent analysis of localized particles only particles with >500 photons were counted as in the "on" state.
Replication	All replication attempts were successful. The exact number of replicates for each experiment is given in the figure legends.
Randomization	We did not perform any randomization as this is a methods paper and randomization was considered to be not necessary for this study.
Blinding	We did not perform any blinding as this is a methods paper and blinding was considered to be not necessary for this study.

Reporting for specific materials, systems and methods

We require information from authors about some types of materials, experimental systems and methods used in many studies. Here, indicate whether each material, system or method listed is relevant to your study. If you are not sure if a list item applies to your research, read the appropriate section before selecting a response.

Materials & experimental systems

n/a	Involved in the study
☒	☐ Antibodies
☒	☐ Eukaryotic cell lines
☒	☐ Palaeontology
☒	☐ Animals and other organisms
☒	☐ Human research participants
☒	☐ Clinical data

Methods

n/a	Involved in the study
☒	☐ ChIP-seq
☒	☐ Flow cytometry
☒	☐ MRI-based neuroimaging